Water Science & Technology

Water Science & Technology Vol 87 No 9, 2195 doi: 10.2166/wst.2023.115

In situ surface modification of forward osmosis membrane by polydopamine/polyethyleneimine-silver nanoparticle for anti-fouling improvement in municipal wastewater treatment

Yan Sun [a,*], Lu Zheng[a], Qianying Feng[a], Xiaoyang Xie[a], Zixin Yong[b], Jiaojie He [a], Liwei Yang[a] and Xiaohong Zhao[a]

[a] School of Civil Engineering, Chang'an University, Xi'an 710061, China
[b] China Northwest Architecture Design and Research Institute Co., Ltd, Xi'an 710018, China
*Corresponding author. E-mail: sunyan2021@chd.edu.cn

YS, 0000-0002-7675-2706; JH, 0000-0003-4267-2908

ABSTRACT

In this work, we demonstrate the surface functionalization of cellulose triacetate membrane with co-deposition of polydopamine (PDA)/polyethyleneimine (PEI) and silver nanoparticles (AgNPs) for antifouling property in municipal wastewater treatment. PDA/PEI was first coated on the membrane surface by single-step co-deposition, while AgNPs were formed *in situ* through catechol groups of PDA immobilizing silver ions and subsequently reducing. The successful surface modification was verified by different membrane characterization techniques. The modified PDA/PEI-nAg CTA membrane exhibits enhanced hydrophilicity and improved antiadhesion and antimicrobial activity. Furthermore, the functional layer had an indistinctive effect on the membrane transport parameters. In addition, dynamic forward osmosis (FO) fouling experiment with raw municipal wastewater as feed solution indicated that the PDA/PEI-nAg CTA membrane exhibited notably lower water flux decrease compared to the nascent CTA membrane. The results of confocal laser scanning microscopy (CLSM) showed that PDA/PEI-nAg CTA membranes effectively reduced the adsorption of organic foulants (proteins and polysaccharides) and inhibited the formation and development of the fouling layer. The membrane surface modification of the CTA membrane with PDA/PEI and AgNPs efficiently mitigated membrane fouling in municipal wastewater treatment.

Key words: antifouling, forward osmosis, municipal wastewater treatment, polydopamine/polyethyleneimine-silver nanoparticle, surface modification

HIGHLIGHTS

- AgNPs were *in situ* immobilized on a CTA FO membrane with PDA/PEI coating layer.
- The PDA/PEI coating and Ag *in situ* generation had no considerable impact on the mass transport coefficients of the CTA FO membrane.
- The PDA/PEI-nAg CTA-modified membrane exhibited excellent antifouling performance for raw municipal wastewater treatment.

GRAPHICAL ABSTRACT

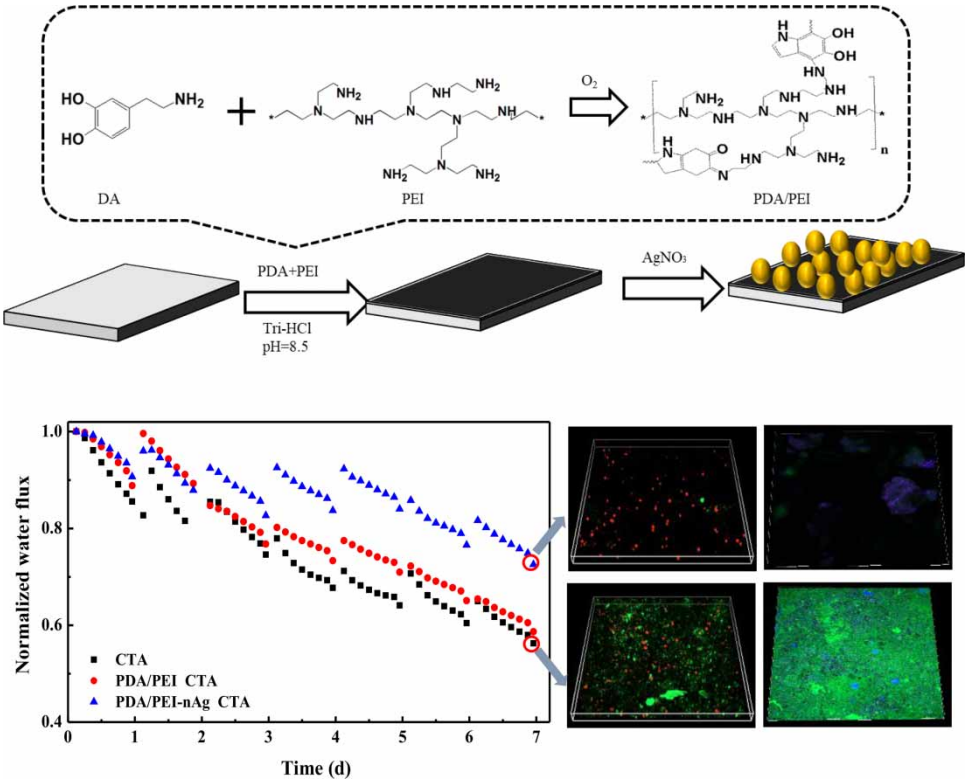

1. INTRODUCTION

Increasing water scarcity and resource depletion with the growing world population become major challenges in the 21st century. To address these problems, membrane-based technology has unique advantages by recovering fresh water and nutrients from municipal wastewater (Yusuf *et al.* 2020). Forward osmosis (FO) is a new burgeoning osmotic pressure-driven membrane separation process, which has obtained wide attention and various applications in wastewater treatment/reclamation, seawater desalination and power generation (Lee & Hsieh 2019; Suwaileh *et al.* 2020). FO relies on the natural osmotic pressure gradient across the membrane to drive water molecules in feed solution (FS) transferring to draw solution (DS) (Goh *et al.* 2019). As a state-of-the-art membrane technology, it is ascribed to its no need for hydraulic pressure, lower membrane fouling propensity as well as high water flux recovery (Wang & Liu 2021).

In spite of its advantages and wide applications, membrane fouling, especially biofouling, remains a major issue for FO, which is ascribed that the membrane is in contact with complex raw wastewater directly during long-term operation (Sun *et al.* 2018; Bao *et al.* 2019; Jung *et al.* 2020). The foulants on the membrane surface give rise to a decrease in water permeability, an increase in the frequency of cleaning and a shortened membrane life (She *et al.* 2016; Ibrar *et al.* 2019). Therefore, various methods are proposed to alleviate membrane fouling, including the pretreatment of FS (Pramanik *et al.* 2019), optimization of operation parameters (Sun *et al.* 2019), cleaning strategies of membranes (Lotfi *et al.* 2018; Kim *et al.* 2020) and modification of membrane (Ibrar *et al.* 2019; Firouzjaei *et al.* 2020).

The membrane surface properties play a fundamental role in membrane fouling control, thus efficient modifications to enhance the fouling resistance of membranes are in high demand (Xu *et al.* 2017). In general, a hydrophilic membrane surface can improve water flux and reduce the adhesion of organic and biological substances so as to enhance the fouling resistance of the membrane surface (Goh *et al.* 2019). Inspired by mussels, the research of dopamine (DA) in forming multi-functional coating on the membrane surface has attracted much attention (Qi *et al.* 2018; Song *et al.* 2018). Under alkaline conditions, dopamine can form a material-independent polydopamine (PDA) coating through self-polymerizing cross-linking (Yang *et al.* 2015). The presence of functional groups in PDA, such as amine, catechol and imine, improves the hydrophilicity of the membrane surface and decreases the adsorption of organic foulants and microorganisms on the

membrane surface (Karkhanechi *et al.* 2014). However, the aggregates are liable to form in the process of self-polymerization, which leads to an inhomogeneous coating and increases the roughness of the membrane surface. In addition, the stability of the PDA layer is insufficient (Yang *et al.* 2016a). Polyethyleneimine (PEI), with superior chemical and thermal stability, is a functional polymer containing abundant amino groups, which can react with PDA through Michael addition and Schiff base reaction, resulting in a smooth and stable PDA/PEI coating in an alkaline environment (Yang *et al.* 2014).

Nevertheless, biofouling cannot be mitigated effectively by the enhancement in membrane hydrophilicity due to the self-replicating ability of live bacteria and the formation of biofilm on the membrane surface (Qi *et al.* 2018; Firouzjaei *et al.* 2020). Modifying the membrane surface with effective biocides is therefore thought to be a good alternative to endow the membrane surface with excellent antibiofouling activity. Most biocides can be classified into three main categories based on different molecular structures: inorganic biocides, organic biocides and organic–inorganic compound biocides. Metal ions such as silver, copper and zinc ions as well as metal oxides like zinc oxide, titanium dioxide and copper oxide are the most common inorganic biocides (Zhu *et al.* 2018). The advantages of inorganic biocides include long-lasting antibacterial effects, a wide range of applications, high heat resistance and easy processing. Nevertheless, some inorganic biocides are usually expensive and do not achieve the desired antimicrobial activity immediately when initially applied. Organic biocides mainly include natural antimicrobial materials such as chitosan and lysozyme and synthetic antimicrobial materials like polyquaterniums and polyquaterniums (Gerba & Müller 2015). Organic biocides tend to have a better bactericidal effect compared to inorganic biocides, while at the same time, they also have obvious disadvantages, such as poor heat resistance, easy decomposition and poor antimicrobial durability. The composite biocides containing both organic and inorganic antimicrobial materials combine the advantages of both organic and inorganic biocides, but its preparation process is relatively complex (Seyedpour *et al.* 2019). Silver nanoparticles (Ag NPs), exhibiting a broad-spectrum antibacterial activity even at low concentrations, were widely employed to be embedded in the membrane surface, which renders the membrane direct, effective and long-lasting antibacterial effect (Zhang *et al.* 2016a). Qiu & He (2018) obtained a long-term antibiofouling membrane via second interfacial polymerization of zwitterion and *in situ* synthesis of Ag NPs by sodium borohydride ($NaBH_4$). However, the preparation of Ag NPs involves additional chemical agents and complicate synthesis procedures, which are time-consuming, cost-ineffective and environment-unfriendly (Zhang *et al.* 2016a). From this viewpoint, PDA/PEI coating layer has enormous potential to reduce the coated silver ions into silver nanoparticles *in situ* due to the strong metal adsorbing and chelating capacities of active groups on PDA/PEI and the great reducibility of dopamine monomer (Yang *et al.* 2016b).

In this study, cellulose triacetate (CTA) FO membrane was coated by PDA/PEI layer to improve the hydrophilicity of the membrane surface and then *in situ* reduction of Ag NPs onto the PDA/PEI coating was aimed to obtain high antibacterial properties. After the modification, the surface morphology, surface chemical composition, surface roughness, surface hydrophilicity and mass transfer performance of membranes were systematically characterized. Besides, the antiadhesion and antibacterial properties of modified membranes against *Escherichia coli* and *Staphylococcus aureus* were experimentally evaluated. Finally, the performance of the modified membrane in the treatment of municipal wastewater was studied and the antifouling mechanism of the modified membrane was revealed by analyzing the type and structure of the fouling layer on the membrane surface.

2. MATERIALS AND METHODS

2.1. Materials and reagents

A CTA membrane was supplied by Hydration Technology Innovations (HTI) as the basis matrix for modification. Dopamine (DA, 98%), polyethyleneimine (PEI, Mw = 600) and tri (hydroxymethyl) amino methane hydrochloride (Tris–HCl, > 99%) were received from Aladdin Reagent Co., Ltd (Shanghai, China) to prepare PDA/PEI coating layer. Silver nitrate ($AgNO_3$) from Sigma-Aldrich (China, Shanghai) was used to form Ag NPs *in situ*. Gram-negative *E. coli* (ATCC25922) and Gram-positive *Staphylococcus aureus* (*S. aureus*, CMCC(B)26003) provided by Luwei Technology Co., Ltd (Shanghai, China) were used for antiadhesion and antibacterial experiments. All reagents in this study used were of analytical grade and deionized water was used in all experiments.

2.2. Surface modification of CTA FO membrane

DA (0.2 g) and PEI (0.3 g) were dissolved in Tris–HCl solution (100 mL, pH = 8.5). The nascent CTA FO membrane was placed on a customized membrane holder with an active layer facing the clean glass plate. This PDA/PEI solution then

was poured into the membrane holder with shaking at 50 rpm for 24 h at room temperature. After reaction, the excessive PDA/PEI solution was removed. The modified membrane was rinsed with DI water and stored in sterile DI water at 4 °C before use. Hereon, the PDA/PEI coated CTA membrane will be designed as PDA/PEI CTA membrane.

After functionalizing the CTA membrane surface of the active layer with PDA/PEI polymers, $AgNO_3$ solution (50 mM) was exposed to the membrane surface to *in situ* form AgNPs with shaking at 50 rpm under dark conditions under room temperature for 5 h. Subsequently, the residual $AgNO_3$ solution was discarded. The modified membrane was rinsed with DI water and stored in sterile DI water at 4 °C before use, referred to as PDA/PEI-nAg CTA membrane. A detailed illustration of CTA membrane modification is shown in Figure 1.

2.3. Membrane characterization

Surface morphologies of the virgin membrane, modified membranes and fouled membranes were identified by scanning electron microscopes (SEM, Model XL 30, Philips, Netherlands) equipped with an energy-dispersive X-ray spectroscope (EDX). The Attenuated Total Reflection-Fourier transform infrared spectroscopy (ATR-FTIR, Spectrum One B, Perkin Elmer Inc, American) analysis was carried out to identify the major functional groups on the surface of virgin, modified and fouled membranes. The chemical composition changes between CTA nascent membrane and modified membranes were characterized by X-ray photoelectron spectroscopy (XPS, K-Alpha, Al Kα radiation). Atomic force microscopy (AFM, BioScope, Veeco Inc.) was employed to measure the membrane surface roughness of the CTA, PDA/PEI CTA and PDA/PEI-nAg CTA membranes and obtain 3D morphological images. The nascent and modified membranes' surface hydrophilicity was evaluated through a water contact angle performed by a contact angle goniometer (SL200B, Solon Tech Co., Ltd, China). The structure and composition of the fouling layer were observed by confocal laser scanning microscopy (CLSM, Nikon C2). The fouled membrane pieces of 0.5×0.5 cm^2 were stained with SYTO 9, PI, fluorescein isothiocyanate (FITC), concanavalin A (Con A) and calcofluor white (CW) in series to label the living bacteria, dead bacteria, proteins, α-D-glucopyranose polysaccharides (α-polysaccharides) and β-D-glucopyranose polysaccharides (β-polysaccharides) in the fouling layer, respectively, and the three-dimensional images were obtained by NIS-Viewer software. The specific steps were provided in the previous literature (Sun *et al.* 2019).

2.4. Evaluation of intrinsic properties

Water permeability coefficient (A) and salt permeability coefficient (B) of the virgin and modified membranes were determined by a reverse osmosis (RO) filtration apparatus (Zhang *et al.* 2016b). Briefly, a membrane with the effective area of 15.89 cm^2 was first compacted with DI water at an applied pressure of 20 bar for 30 min. Until the water flux became stable, the value A was calculated according to Equation (1). Subsequently, under the same conditions, the salt rejection (R_s) was determined based on measuring conductivity by replacing DI water with 20 mM NaCl, and calculated using Equation (2). Therefore, according to the dissolution–diffusion theory (Tang *et al.* 2010), the salt permeability coefficient

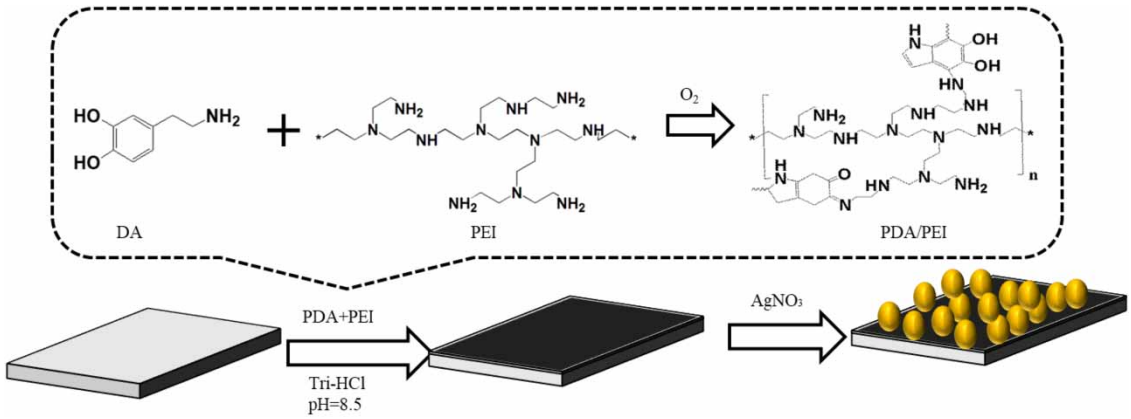

Figure 1 | Schematic illustration of CTA membrane modification by coating PDA/PEI and *in situ* Ag NPs synthesis on the membrane surface.

of the modified membranes was calculated from A and R_s as shown in Equation (3).

$$A = \frac{J_w}{\Delta P} \tag{1}$$

$$R_s = \left(1 - \frac{C_{p-s}}{C_{f-s}}\right) \times 100\% \tag{2}$$

$$\frac{100 - R_s}{R_s} = \frac{B}{A(\Delta P - \Delta \pi)} \tag{3}$$

where J_w (L/(m^2·h)) is the water flux with the DI water as feed solution in RO test; ΔP (bar) is the applied trans-membrane hydraulic pressure; C_{p-s} and C_{f-s} (mg/L) are the salt concentrations of the permeate and feed solutions; $\Delta \pi$ (Pa) is an osmotic pressure difference.

2.5. Antifouling property evaluation

2.5.1. Antiadhesion property tests

Anti-adhesive tests were conducted to observe the attached cells on the fouled membranes by SEM. In brief, after sterilizing with an ultraviolet lamp for 15 min, small pieces (1 × 1 cm) of virgin membrane and modified membranes were kept in contact with 5 mL *E. coli* and *S. aureus* suspension ($10^8 \sim 10^9$ CFU/mL), respectively, for 12 h at 37 °C, and then gently washed with phosphate-buffered solution (PBS, pH = 7.5) to remove the loosely attached bacteria. Chemical fixation pretreatment of the fouled membranes was then carried out by the method described by Xiong *et al*. (2016) to observe the adhesion of bacteria on the membrane surface.

2.5.2. Antibacterial property tests

The diffusion inhibition zone method was employed to evaluate the bacterial inhibition behaviors of the modified membranes. Briefly, 200 μL bacterial suspension (*E. coli* and *S. aureus*) was spread on an LB medium. The active layer of membrane coupons (the original membrane and the modified membranes) with a diameter of 10 mm was contacted with bacteria and incubated at 37 °C for 24 h. The size of the inhibition zone around the samples was determined to characterize the antibacterial activity.

The antibacterial property of the modified membrane was further evaluated by the colony-forming unit. A small piece (1 × 1 cm) of each membrane was kept in contact with 5 mL *E. coli* and *S. aureus* suspension, respectively, for 24 h at 37 °C while shaking at 100 rpm. The membranes were then taken out and washed with PBS to remove the free cells from the membrane surface. After rinsing, the membranes were immersed in 0.85% sterilized normal saline (5 mL) for 5 min with sonication and vortex to remove the attached bacteria from the membrane surface and dissolve in the solution. The suspension (1 mL) after serially diluted was inoculated in LB agar medium, and the colonies of viable bacteria on the membrane surface were counted after inoculating for 24 h at 37 °C.

2.5.3. Dynamic antifouling experiments

The dynamic fouling experiment was performed by the laboratory-scale FO system with cross-flow side stream configuration run in parallel (Fig. S1). Co-current recirculation of the FS and DS was employed on each side of the membrane module (length × width × height = 10 cm × 4 cm × 0.3 cm) by two peristaltic pumps. The effective FO membrane area was 20 cm^2. In order to evaluate the antifouling performance of modified membranes in more realistic settings, raw municipal wastewater was adopted as a feed solution in the dynamic fouling experiment, which was obtained from the septic tank effluent in the adjacent residential area. Prior to use, municipal wastewater was filtered with a 200 mesh screen and the wastewater displayed the following main quality: 150 ~ 280 mg/L chemical oxygen demand (COD), 35 ~ 60 mg/L ammonia nitrogen (NH_4^+-N), 38 ~ 70 mg/L total nitrogen (TN) and 1 ~ 4 mg/L phosphate (PO_4^{3-}-P) (more detailed information illustrated in Table S1). The standard synthetic seawater was prepared as a DS according to the detailed composition listed in Table S2.

The pristine and modified membranes were installed with the active layer directly facing the municipal wastewater (FS) and the support layer in contact with the synthetic seawater (DS). Firstly, a baseline experiment was carried out using DI as FS and 2 L synthetic seawater was used as DS for 24 h. Subsequently, the FS was replaced with raw municipal wastewater with avolume of 1 L. The system was operated for 7 days with across-flow velocity of 10 cm/s. A stirring device was adopted to provide mixing in the FS tank. And the DS tank was located on a digital balance (Sartorius, BSA3202S) in order to calculate

the membrane flux based on the weight changes of the DS with the extension of the operation time. At the end of every day, the FS and DS were replaced with fresh ones to avoid significant changes in their concentrations. All experiments were carried out at room temperature. Water samples were collected from every day detected on the basis of the Chinese NEPB standard methods (CEPB 2002). The dynamic antifouling performance of the modified membrane in the treatment of raw municipal sewage was discussed by analyzing the flux change and the structure and composition of fouling layer on the membrane surface.

3. RESULT AND DISCUSSION

3.1. Membrane surface characterization

3.1.1. Surface morphology analysis

The surface morphologies of the active layer of the virgin CTA membrane, PDA/PEI CTA membrane and PDA/PEI-n Ag CTA membrane were characterized by SEM. As exhibited in Figure 2, a relatively smooth active surface could be found on the virgin CTA membrane. After the deposition of PDA/PEI, a polymer layer could be clearly observed on the membrane surface (Figure 2(b)). It indicates that PDA/PEI was successfully coated on the surface of the pristine CTA membrane. After *in situ* formation of AgNPs by the reducibility of adjacent phenolic hydroxyls of PDA, the spherical nanoparticles of AgNPs on the membrane surface were noticeable. Furthermore, AgNPs immobilized were demonstrated by the EDX elemental-mapping, indicating that AgNPs were distributed homogeneously throughout the modified membrane surface (Figure 2(c)).

3.1.2. Elemental composition analysis

Figure 3(a) shows the changes of functional groups on the membrane surface before and after modification verified by ATR-FTIR spectroscopy. It was obvious that four sharp peaks could be observed for the virgin membrane at 1,738, 1,652, 1,367, 1,215 and 1,033 cm^{-1}, respectively, which were attributed to the chemical structure of CTA (Sun *et al.* 2019). Compared with the virgin CTA membrane, no obvious peaks were found on the modified membranes surface. It is because the characteristic absorption peaks of the virgin CTA membrane and PDA/PEI coating layer were at 1,700–1,500 cm^{-1} (Chew *et al.* 2017). The absorption peaks assigned to phenolic –O–H bending and stretching vibration of PDA were at 1,368 cm^{-1} (Karkhanechi *et al.* 2014). And the signal assigned to the stretching vibration of N–H of the primary amines of PEI was at 1,650 cm^{-1} (Zhu *et al.* 2017). Thus, the absorption peaks of the functional groups in the ATR-FTIR spectra of the membrane surface before and after the modification were quite similar.

The elementary composition change of the CTA membrane surface after modification was further analyzed by XPS to elucidate the structure of the membrane surface precisely. As shown in Figure 3(b), after the PDA/PEI deposition, an absorption peak of N element (396.6 eV) emerged. It indicated that PDA/PEI with substantial amino groups was introduced to the membrane surface successfully. As for PDA/PEI-n Ag CTA membrane, not only the absorption peak of N element but also a new peak with the binding energy of 365.1 eV corresponding to Ag 3d appeared on the membrane surface (Yang *et al.* 2016b). This peak verified that the silver ions were fixed and then reduced to Ag NPs *in situ* successfully on the membrane surface by the catechol groups of the PDA/PEI coating layer.

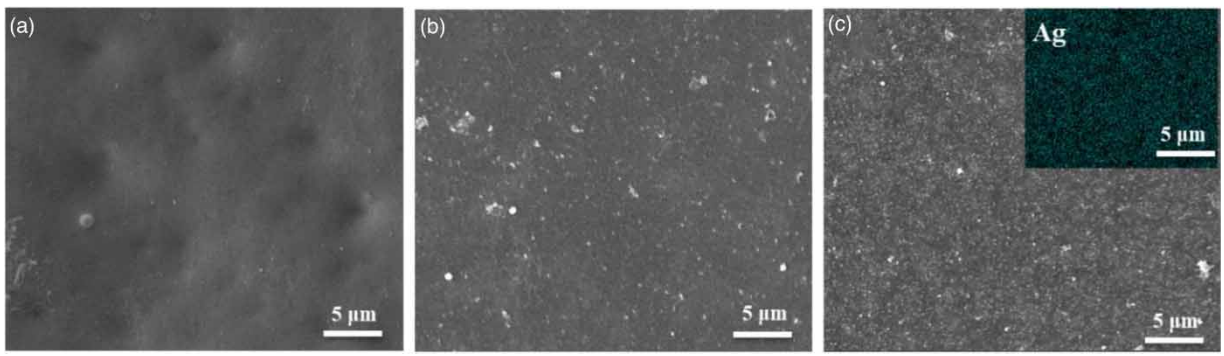

Figure 2 | The surface morphology of the active layer of virgin CTA membrane (a), PDA/PEI CTA membrane (b,c) SEM and mapping image of PDA/PEI-n Ag CTA membrane.

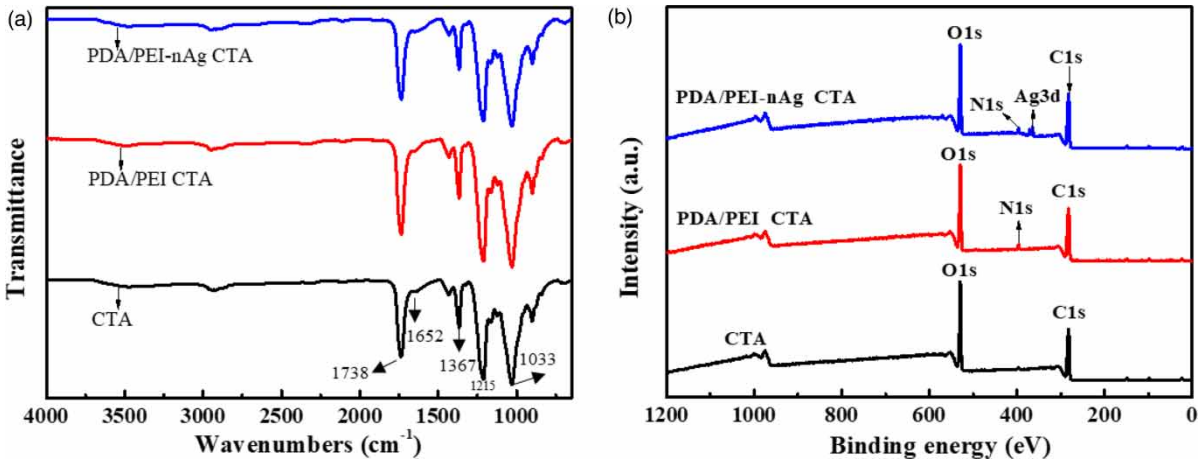

Figure 3 | ATR-FTIR (a) and XPS (b) spectra of the virgin CTA membrane, PDA/PEI CTA membrane and PDA/PEI-n Ag CTA membrane.

3.1.3. Surface roughness analysis

The surface roughness of the prepared membranes was investigated by AFM. The AFM 3D images and corresponding roughness analysis results of the various membranes in terms of Rq and Ra are shown in Figure 4. According to the AFM results, the roughness of the membrane increased after coating PDA/PEI layer, as Rq changed from 3.33 to 8.74 nm and Ra increased

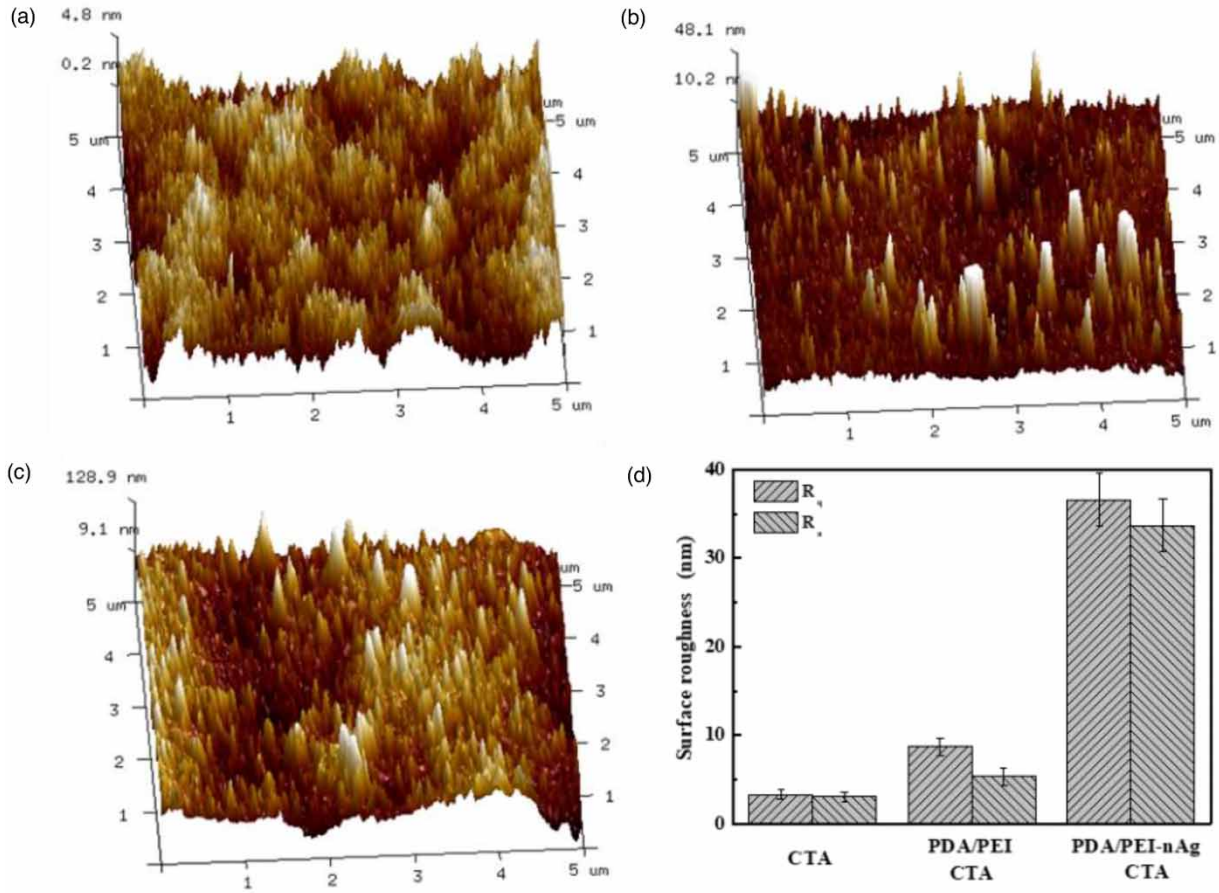

Figure 4 | AFM 3D images for virgin CTA membrane (a), PDA/PEI CTA membrane (b), PDA/PEI-n Ag CTA membrane (c,d) surface roughness determined by AFM.

from 3.06 to 5.41 nm. Although the reaction between PEI and PDA reduced the non-covalent interactions in the PDA polymer, there were still a few aggregates on the membrane surface, as shown in Figure 2(b). It resulted in an increase in the roughness of the modified membranes. In addition, compared with the virgin CTA membrane, the average roughness of the PDA/PEI-n Ag CTA membrane was increased to 36.6 nm owing to the deposition of abundant Ag NPs on the membrane surface.

3.1.4. Surface hydrophilicity analysis

In order to discuss the hydrophilicity of the virgin and modified CTA membrane, the measurement of water contact angles was conducted. As presented in Fig. S2, the water contact angle value dropped from 69.5° to 45.3° after modification by PDA/PEI coating, indicating an enhancement of surface hydrophilicity. It was attributed to the introduction of various hydrophilic functional groups by PDA/PEI coating, such as amino and hydroxyl functional groups. After the *in situ* reduction of AgNPs on the membrane surface which led to a decreased water contact angle, the hydrophilicity of the PDA/PEI-n Ag CTA membrane was further improved due to the hydrophilic properties of silver nanoparticles.

3.2. Intrinsic separation properties of the membranes

The mass transport coefficients, including the water permeability coefficient (A) and the salt permeability coefficient (B), were important property of the membrane. As summarized in Figure 5, in comparison with the A value (0.51 ± 0.01 L/(m^2·h·bar)) and B value (0.50 ± 0.02 L/(m^2·h)) of the virgin CTA membrane, the water permeability coefficient (0.48 ± 0.01 L/(m^2·h·bar)) and salt permeability coefficient (0.42 ± 0.02 L/(m^2·h)) of the membrane after coating PDA/PEI were slightly reduced, which was due to the additional transfer resistance from PDA/PEI coating layer. And the slight reduction value was because of the relatively thin PDA/PEI coating layer. After the *in situ* formation of Ag NPs on the membrane surface, the values A and B were 0.46 ± 0.01 L/(m^2·h·bar) and 0.50 ± 0.02 L/(m^2·h), respectively. The PDA/PEI layer and the membrane holes were blocked by Ag NPs to some extent, which reduced the water permeability of the membrane, but increased the rejection rate of salt at the same time. The results illustrated that the modification of the CTA membrane by PDA/PEI coating and Ag generation had no considerable effect on the mass transfer performance and integrity of the membrane.

3.3. Antibiofouling properties of the membranes

3.3.1. The antiadhesion property

Bacteria tend to adhere to the membrane surface and use the surrounding nutrients to reproduce to form the biofilm on the membrane surface, thus affecting the operating performance of the membrane. Therefore, to improve the antifouling performance of the membrane, the rate of bacteria attached to the membrane surface should first be reduced. Figure S3 shows the

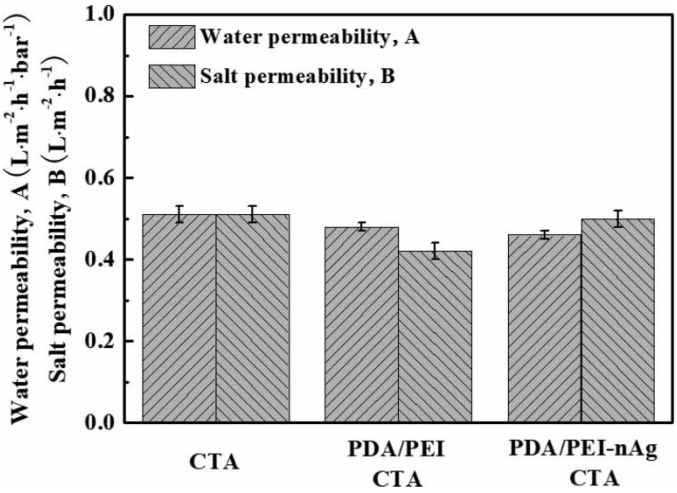

Figure 5 | Transport properties of virgin CTA membrane, PDA/PEI CTA membrane and PDA/PEI-n Ag CTA membrane.

adhesion of *E. coli* and *S. aureus* on the CTA membrane, PDA/PEI CTA membrane and PDA/PEI-n Ag CTA membrane determined by SEM.

As demonstrated in Fig. S3, the number of *E. coli* attached to modified CTA membranes was decreased in comparison with the pristine CTA membrane. Furthermore, the *E. coli* attached on the surface of the PDA/PEI-nAg CTA-modified membrane was significantly deformed. *S. aureus* almost covered evenly the surface of the pristine CTA membrane. In contrast, the number of *S. aureus* on the PDA/PEI CTA membrane surface was greatly reduced due to the improvement of hydrophilicity. However, by SEM observation, the number of *S. aureus* attached to the PDA/PEI CTA membrane surface was not remarkably lower due to the higher roughness. The results revealed that the better bacterial adhesion resistance of the PDA/PEI CTA membrane and PDA/PEI-n Ag CTA membrane was attributed to the improved hydrophilicity of membranes to some extent.

3.3.2. The antibacterial property

The antibacterial properties of the modified membranes were evaluated by the diffusion inhibition zone test with *E. coli* and *S. aureus* as model bacteria first. As seen from Figure 6, no obvious inhibition zone appeared around the virgin CTA membrane and PDA/PEI CTA membrane. But inhibition zones against *E. coli* and *S. aureus* with the diameters of 13 and 12 mm were observed around the PDA/PEI-n Ag CTA membrane, indicating that PDA/PEI-n Ag successfully endowed the CTA membrane with the antibacterial ability.

Furthermore, the number of viable bacterial colonies adhering to the membrane's surface is also shown in Figure 6. The percentages of bacterial content in Figure 6 were based on the number of viable bacterial colonies on the surface of the original CTA membrane. After the deposition of PDA/PEI, the viable bacterial colonies of *E. coli* and *S. aureus* on the membrane surface decreased by 6 and 10%, respectively, which was in agreement with the results obtained from the SEM images (Fig. S3). It was due to the increased hydrophilicity of the membrane surface leading to reduce the adhesion of bacteria. The relative content of viable bacteria colonies on the surface of the PDA/PEI-n Ag decorated membrane was greatly decreased, and the mortality rates of *E. coli* and *S. aureus* were reaching about 90 and 85%, respectively. It was ascribed that the introduction of Ag NPs on the modified membrane surface. Ag NPs can directly contact bacteria and permeate into cells, resulting in inactivating important cellular functions. Furthermore, Ag NPs could release silver ions in contact with the bacterial suspension. And then Ag^{+} could destroy the cellular membrane or even permeate inside the bacteria, interfering with the normal metabolism of the bacteria followed by the death of the bacteria (Zhang *et al.* 2016a). As mentioned in section 3.3.1, the overall structure of the cell had been destroyed (Fig. S3). Therefore, the immobilization of Ag NPs on the PDA/PEI-n Ag modified membrane surface endowed the membrane with superior antibacterial property toward *E. coli* and *S. aureus*.

3.4. The dynamic antifouling performance of modified membranes

3.4.1. Membrane flux analysis and process performance

To further evaluate the antifouling property of PDA/PEI-n Ag CTA membrane, the actual municipal wastewater was used as FS operated for 7 days. The normalized water flux decline patterns of the virgin and modified membranes are shown in

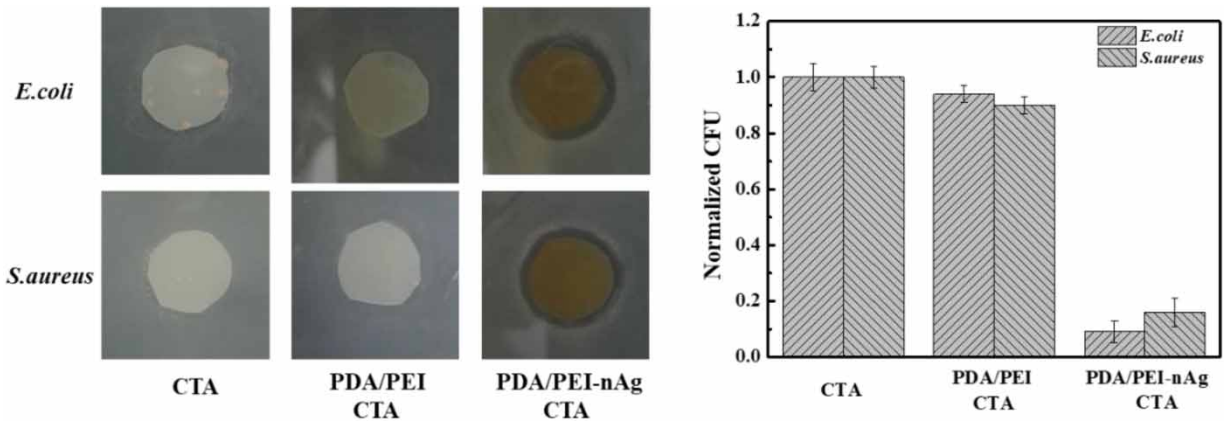

Figure 6 | Diffusion inhibition zone and antimicrobial properties of CTA, PDA/PEI CTA and PDA/PEI-n Ag CTA after exposure to *E. coli* and *S. aureus*.

Figure 7. As can be seen, the trend of the normalized flux decline of all the membranes showed great consistency on the first day. A significant flux reduction was observed for the original CTA membrane during the operation, which was decreased to 56.3% of the initial flux at the end of 7 days. And a slightly higher flux was obtained by the PDA/PEI CTA membrane due to the increased hydrophilicity of the membrane surface. After the operation, the flux decline of the PDA/PEI CTA membrane was 27.4%. By contrast, the flux of PDA/PEI-n Ag CTA membrane was obviously higher than that of the original CTA membrane and the PDA/PEI CTA membrane during the operation. The final flux was 72.6% of the initial flux. Furthermore, after the change of fresh FS and DS every day, the daily initial flux and the average flux of PDA/ PEI-n Ag CTA membrane were significantly improved. It indicated that the membrane surface modification of the original CTA membrane by coating with PDA/PEI and introducing silver nanoparticles *in situ* could effectively alleviate the membrane fouling and thus enhance the water permeate flux in the actual municipal sewage treatment. The process performance for pollutant removal is summarized in Fig. S4. As can be seen, both the original CTA membrane and the modified CTA membrane achieved excellent removal for COD, and the effluent concentration of COD was below 20 mg/L. The removal efficiency for NH_4^+-N was only about 60% due to its low molecular weight and positive charge. However, it was noteworthy that the concentration of PO_4^{3-}-P in the DS was almost undetectable in both virgin and modified CTA membrane systems.

3.4.2. Analysis of functional groups in fouling layer

Surface functional groups of the fouled FO membranes were analyzed through ATR-FTIR to identify the components of organic foulants formed as shown in Figure 8. As mentioned in Section 3.1.2, the absorption peaks of virgin CTA membrane, PDA/PEI CTA membrane and PDA/PEI-n Ag CTA membrane were similar, so only the FTIR spectra of virgin CTA membrane and the fouled membranes were selected for analysis in this section. It could be noted that the specific peaks at 1,738, 1,368, 1,214 and 1,035 $cm^{-1}$of virgin CTA membrane almost disappeared completely at the end of the membrane fouling test (Figure 8(a)) (Zhang *et al.* 2016a). However, the new absorption peaks of the fouled membranes appeared, indicating the surface of the virgin membrane and modified membranes were covered by a fouling layer (Figure 8(b)). Signals at 1,634 and 1,535 cm^{-1} were associated with the stretching vibration of C = O (amide I peak), the bending vibration of N – H (amide II peak) and the stretching vibration of C – N (amide III peak), representing the presence of proteins or proteinaceous substances (Bao *et al.* 2019). A sharp absorption peak at 1,018 cm^{-1} was indicative of the presence of polysaccharides (Sun *et al.* 2016). These results revealed that the organic foulants of the fouling layer were mainly polysaccharides and proteins. In addition, the peak intensities of the modified membranes were weaker than the virgin membrane. Extracellular polymeric substances (EPS) play an important role in the formation and development of the biofouling layer (Bogler *et al.* 2017). The main components of EPS are protein and polysaccharide, which account for 70 ~ 80% of the total concentration. In the initial formation of biofouling, EPS is firstly deposited on the FO membrane surface facilitating the attachment of bacteria. After that, the dramatic increase in the clusters of EPS associated with bacteria lead to the growth and development of the biofouling layer (Yuan *et al.* 2015). The non-covalent bond network structure between polysaccharide and protein makes the membrane fouling mechanism more complicated, accelerates the formation of irreversible fouling and shortens the service

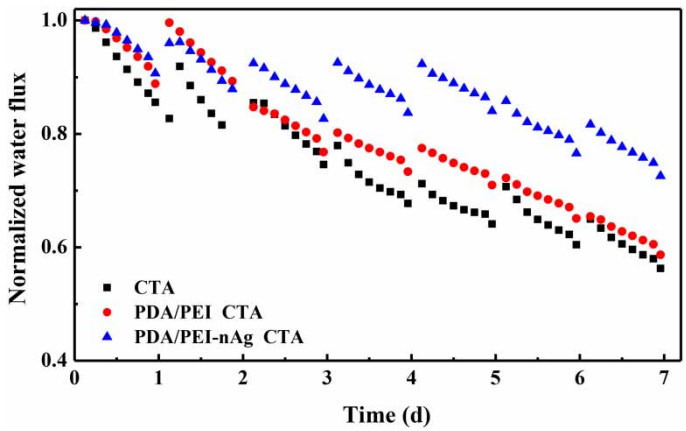

Figure 7 | Normalized water flux decline patterns for virgin CTA membrane, PDA/PEI CTA membrane and PDA/PEI-n Ag CTA membrane.

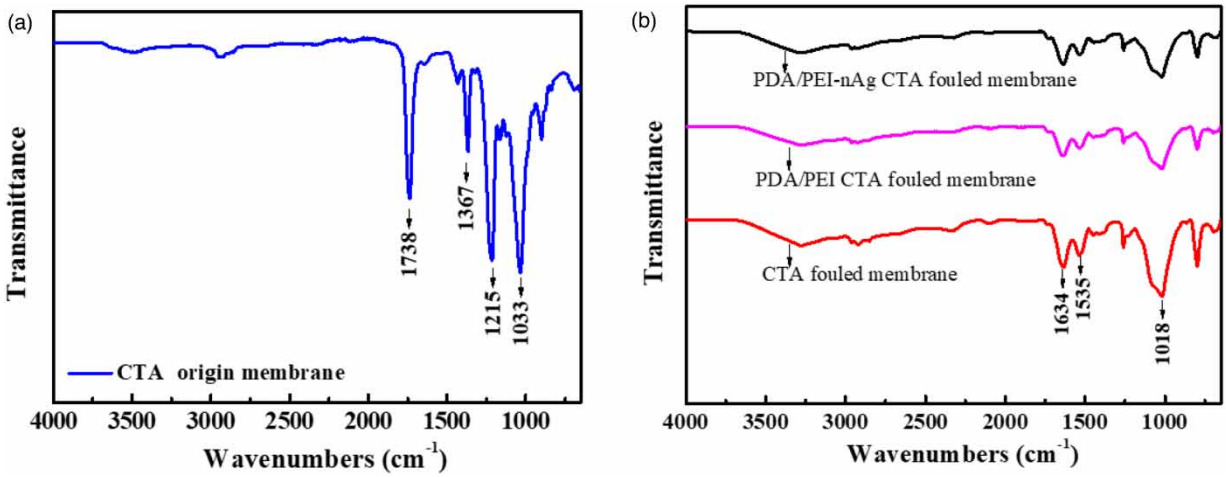

Figure 8 | ATR-FTIR spectra of membrane surfaces: (a) virgin CTA membrane and (b) fouling layer in the surface of virgin CTA, PDA/PEI CTA and PDA/PEI-n Ag CTA.

life of the membrane (Neemann *et al.* 2013). It might be concluded that the modified membranes could reduce the accumulation of organic foulants to mitigate membrane fouling during the treatment of municipal wastewater.

3.4.3. Analysis of biofouling layer on membrane surface

To precisely understand the mechanism of modified membrane fouling control, the composition and structure of the fouling layer on the fouled membrane surface were investigated by the CLSM. Figure 9 shows the distribution of living bacteria (green) and dead bacteria (red) on the fouled membrane surface. Compared to the modified membranes, active bacteria were much more abundant in the virgin membrane surface, while some dead bacteria were still observed due to the metabolism of bacteria during the process of forming a biofilm. However, relatively few active bacteria accumulated on the fouling layer of PDA/PEI CTA membrane, due to the improvement of membrane hydrophilicity as mentioned above. In addition, the number and distribution of dead bacteria increased significantly on the fouled PDA/PEI-nAg CTA membrane, indicating that most bacteria attached to the membrane surface were killed by Ag NPs.

The number of living bacteria in the biofilm formed on the fouled surface of virgin CTA, PDA/PEI CTA and PDA/PEI-n Ag CTA membrane was further determined by plate counting method, and the concentrations of viable bacteria are displayed in Fig. S5. It was found that the concentrations of viable bacteria on the surface of virgin CTA, PDA/PEI CTA

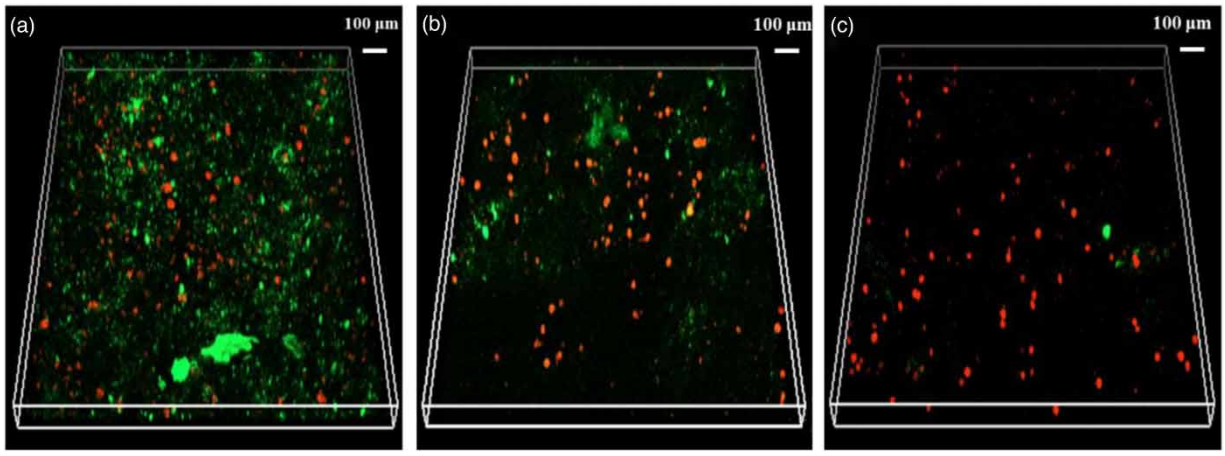

Figure 9 | CLSM images of live/dead cells in the fouling layer of (a) virgin CTA, (b) PDA/PEI CTA and (c) PDA/PEI-n Ag CTA. Please refer to the online version of this paper to see this figure in colour: http://dx.doi.org/10.2166/wst.2023.115.

and PDA/PEI-nAg CTA membrane were $(11.7 \pm 1.56) \times 10^5$, $(7.1 \pm 0.14) \times 10^5$ and $(1.3 \pm 0.5) \times 10^5$ CFU/mL, respectively. The observations were in accordance with the results of CLSM results. These results demonstrated that the introduction of Ag NPs based on the secondary reaction platform of PDA/PEI coating could inhibit the formation and development of biofilm on the membrane surface.

During the process of metabolism, the live bacteria in the fouling layer can secrete extracellular polymers, such as polysaccharides and proteins, which is consistent with the main organic foulants on the membrane surface as shown in Figure 8. Therefore, in order to further explore the structure and composition of the fouling layer on the membrane surface, the proteins (green), α-polysaccharides (purple) and β-polysaccharides (blue) were investigated by the CLSM, as summarized in Figure 10. As for the virgin CTA membrane, abundant proteins formed a relatively uniform coating layer on the fouled

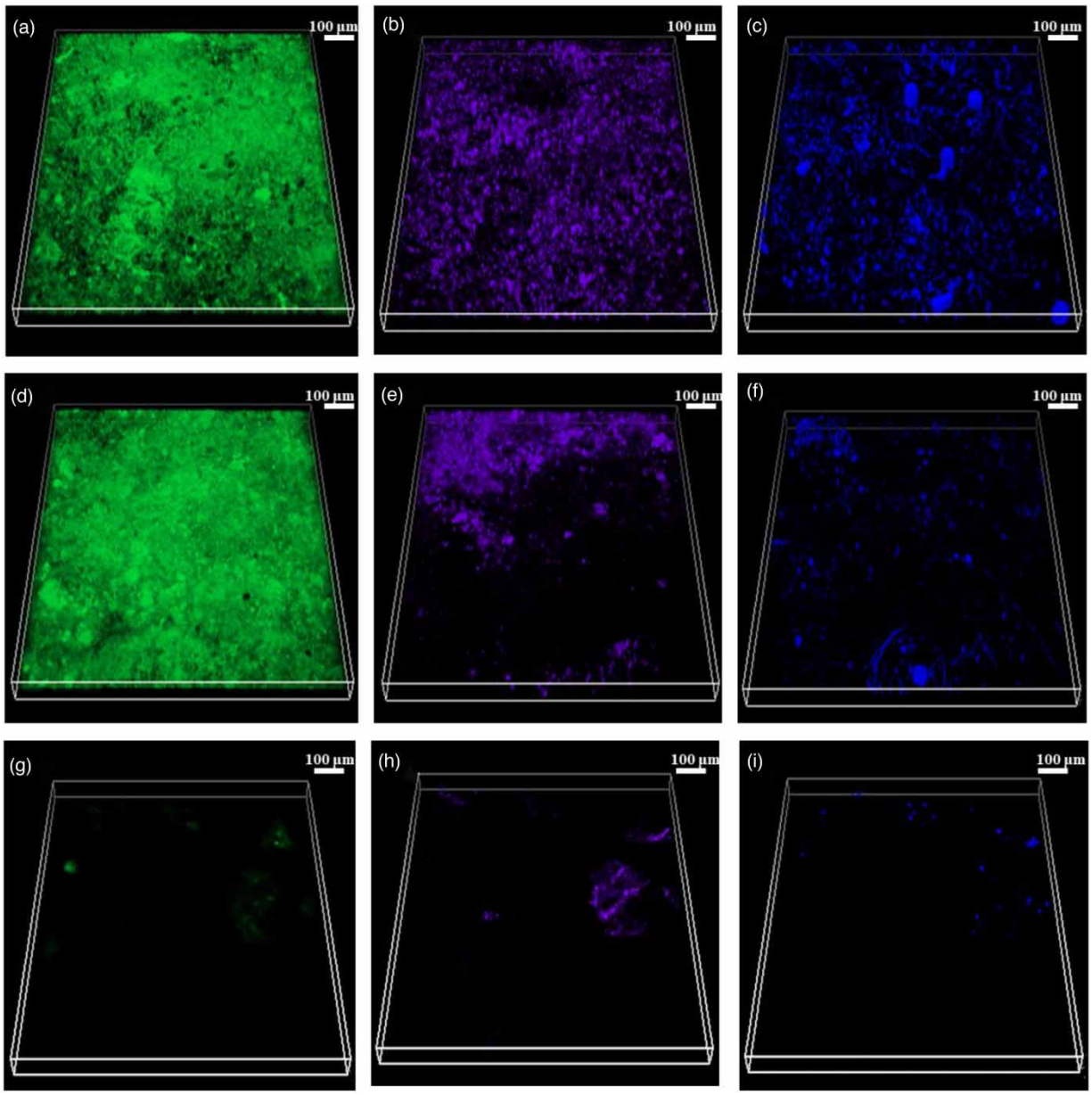

Figure 10 | CLSM images of the foulants on the fouled membranes of virgin CTA ((a) proteins; (b) α-D-glucopyranose polysaccharides and (c) β-D-glucopyranose polysaccharides), PDA/PEI CTA ((d) proteins; (e) α-D-glucopyranose polysaccharides and (f) β-D-glucopyranose polysaccharides) and PDA/PEI-n Ag CTA ((g) proteins; (h) α-D-glucopyranose polysaccharides and (i) β-D-glucopyranose polysaccharides), respectively. Please refer to the online version of this paper to see this figure in colour: http://dx.doi.org/10.2166/wst.2023.115.

membrane surface. And α-polysaccharides existed as uniform aggregates, while β-polysaccharides unevenly covered the entire fouled membrane surface. As for PDA/PEI CTA membrane, the distribution of proteins was similar to that of the virgin CTA, while α-polysaccharides and β-polysaccharides only localized on the part of the membrane surface as aggregates. By comparison, the distribution and abundance of proteins, α-polysaccharides and β-polysaccharides on the membrane surface decreased, and only litter clusters were observed on PDA/PEI-n Ag CTA fouled membrane.

Increase in the hydrophilicity of the membrane surface can form a hydrophilic hydration layer, which can generate a steric hindrance effect and energy barrier to prevent the adsorption and deposition of hydrophobic foulants. However, the function of hydrophilic materials cannot effectively kill the bacteria that have attached to the membrane surface, which can rapidly reproduce and form biofilm under appropriate conditions leading to severe biofouling. Therefore, to effectively control membrane fouling, it is essential to endow the membrane surface with antiadhesion and antibiofouling abilities simultaneously. Based on the analysis of the above experimental results, a variety of hydrophilic functional groups, such as catechol, and amino, introduced by the PDA/PEI could reduce the deposition of foulants and bacteria (Figures 9 and 10). The *in situ* formation of silver nanoparticles by the reducibility of PDA could further improve the hydrophilic and antimicrobial properties of the membrane surface to control the formation and development of biofilm and mitigate membrane fouling efficaciously.

4. CONCLUSION

In this work, PDA/PEI was coated on the surface of the CTA membrane, followed by the *in situ* reduction of AgNPs to obtain the high antifouling and antibacterial PDA/PEI-nAg CTA membrane. The hydrophilicity of the PDA/PEI-n Ag CTA membrane was significantly improved without affecting the mass transport and integrity. After exposure to *E. coli* and *S. aureus* for 24 h, the PDA/PEI-nAg CTA membrane displayed superior antibacterial properties with the bactericidal ratio reaching 90 and 85%, respectively. In dynamic fouling experiments for municipal wastewater treatment, the decline of water flux of PDA/PEI-n Ag CTA membrane was significantly reduced, and the number of viable bacteria and organic substances attached to the membrane surface was remarkably decreased in comparison with the virgin CTA membrane. This facile and eco-friendly membrane surface modification approach has great potential in mitigating the FO membrane fouling.

ACKNOWLEDGEMENTS

The authors gratefully acknowledge the financial support from Science and Technology Project of Shaanxi Province, China (Grant No. 2021JQ-222) and the Young Talent fund of University Association for Science and Technology in Shaanxi, China (Grant No. 20200413).

DATA AVAILABILITY STATEMENT

All relevant data are included in the paper or its Supplementary Information.

CONFLICT OF INTEREST

The authors declare there is no conflict.

REFERENCES

Bao, X., Wu, Q. L., Tian, J. Y., Shi, W. X., Wang, W., Zhang, Z. Q., Zhang, R. J., Zhang, B., Guo, Y., Shu, S. H. & Cui, F. Y. 2019 Fouling mechanism of forward osmosis membrane in domestic wastewater concentration: role of substrate structures. *Chemical Engineering Journal* **370**, 262–273.

Bogler, A., Lin, S. H. & Bar-Zeev, E. 2017 Biofouling of membrane distillation, forward osmosis and pressure retarded osmosis: principles, impacts and future directions. *Journal of Membrane Science* **542**, 378–398.

CEPB 2002 *Standard Methods for the Examination of Water and Wastewater*. Chinese Environmental Science Press, China.

Chew, N. G. P., Zhao, S., Malde, C. & Wang, R. 2017 Superoleophobic surface modification for robust membrane distillation performance. *Journal of Membrane Science* **541**, 162–173.

Firouzjaei, M. D., Seyedpour, S. F., Aktij, S. A., Giagnorio, M., Bazrafshan, N., Mollahosseini, A., Samadi, F., Ahmadalipour, S., Firouzjaei, F. D., Esfahani, M. R., Tiraferri, A., Elliott, M., Sangermano, M., Abdelrasoul, A., McCutcheon, J. R., Sadrzadeh, M., Esfahani, A. R. & Rahimpour, A. 2020 Recent advances in functionalized polymer membranes for biofouling control and mitigation in forward osmosis. *Journal of Membrane Science* **596**, 117604.

Gerba, C. P. & Müller, V. 2015 Quaternary ammonium biocides: efficacy in application. *Applied and Environmental Microbiology* **81** (2), 464–469.

Goh, P. S., Ismail, A. F., Ng, B. C. & Abdullah, M. S. 2019 Recent progresses of forward osmosis membranes formulation and design for wastewater treatment. *Water* **11** (10), 2043.

Ibrar, I., Naji, O., Sharif, A., Malekizadeh, A., Alhawari, A., Alanezi, A. A. & Altaee, A. 2019 A review of fouling mechanisms, control strategies and real-time fouling monitoring techniques in forward osmosis. *Water* **11** (4), 695.

Jung, J., Ryu, J., Yu, Y. & Kweon, J. 2020 Characteristics of organic fouling, reversibility by physical cleaning and concentrates in forward osmosis membrane processes for wastewater reclamation. *Chemosphere* **245**, 125787.

Karkhanechi, H., Takagi, R. & Matsuyama, H. 2014 Biofouling resistance of reverse osmosis membrane modified with polydopamine. *Desalination* **336**, 87–96.

Kim, Y. J., Li, S. & Ghaffour, N. 2020 Evaluation of different cleaning strategies for different types of forward osmosis membrane fouling and scaling. *Journal of Membrane Science* **596**, 117731.

Lee, D. J. & Hsieh, M. H. 2019 Forward osmosis membrane processes for wastewater bioremediation: research needs. *Bioresource Technology* **290**, 121795.

Lotfi, F., Samali, B. & Hagare, D. 2018 Cleaning efficiency of the fouled forward osmosis membranes under different experimental conditions. *Journal of Environmental Chemical Engineering* **6** (4), 4555–4563.

Neemann, F., Rosenberger, S., Jefferson, B. & Mcadam, E. J. 2013 Non-covalent protein–polysaccharide interactions and their influence on membrane fouling. *Journal of Membrane Science* **446**, 310–317.

Pramanik, B. K., Shu, L., Jegatheesan, V. & Bhuiyan, M. A. 2019 Effect of the coagulation/persulfate pre-treatment to mitigate organic fouling in the forward osmosis of municipal wastewater treatment. *Journal of Environmental Management* **249**, 109394.

Qi, L. B., Hu, Y. X., Liu, Z. Y., An, X. C. & Bar-Zeev, E. 2018 Improved anti-biofouling performance of thin-film composite forward-osmosis membranes containing passive and active moieties. *Environmental Science & Technology* **52** (17), 9684–9693.

Qiu, M. & He, C. J. 2018 Novel zwitterion-silver nanocomposite modified thin-film composite forward osmosis membrane with simultaneous improved water flux and biofouling resistance property. *Applied Surface Science* **455**, 492–501.

Seyedpour, S. F., Rahimpour, A. & Najafpour, G. 2019 Facile in-situ assembly of silver-based mofs to surface functionalization of tfc membrane: a novel approach toward long-lasting biofouling mitigation. *Journal of Membrane Science* **573**, 257–269.

She, Q. H., Wang, R., Fane, A. G. & Tang, C. Y. Y. 2016 Membrane fouling in osmotically driven membrane processes: a review. *Journal of Membrane Science* **499**, 201–233.

Song, H.-m., Zhu, L.-j., Zeng, Z.-x. & Xue, Q.-j. 2018 High performance forward osmosis cellulose acetate (CA) membrane modified by polyvinyl alcohol and polydopamine. *Journal of Polymer Research* **25** (7), 1–8.

Sun, Y., Tian, J. Y., Zhao, Z. W., Shi, W. X., Liu, D. M. & Cui, F. Y. 2016 Membrane fouling of forward osmosis (FO) membrane for municipal wastewater treatment: a comparison between direct FO and OMBR. *Water Research* **104**, 330–339.

Sun, Y., Tian, J. Y., Song, L. M., Gao, S. S., Shi, W. X. & Cui, F. Y. 2018 Dynamic changes of the fouling layer in forward osmosis based membrane processes for municipal wastewater treatment. *Journal of Membrane Science* **549**, 523–532.

Sun, Y., Gao, S. S., Tian, J. Y., Hao, X. J., Liu, Z. Q., Shi, W. X. & Cui, F. Y. 2019 Air bubbling for membrane fouling control in a submerged direct forward osmosis system for municipal wastewater treatment. *Environmental Science-Water Research & Technology* **5** (4), 684–692.

Suwaileh, W., Pathak, N., Shon, H. & Hilal, N. 2020 Forward osmosis membranes and processes: a comprehensive review of research trends and future outlook. *Desalination* **485**, 114455.

Tang, C. Y. Y., She, Q. H., Lay, W. C. L., Wang, R. & Fane, A. G. 2010 Coupled effects of internal concentration polarization and fouling on flux behavior of forward osmosis membranes during humic acid filtration. *Journal of Membrane Science* **354** (1–2), 123–133.

Wang, J. & Liu, X. 2021 Forward osmosis technology for water treatment: recent advances and future perspectives. *Journal of Cleaner Production* **280**, 124354.

Xiong, J. L., Fu, D. F., Singh, R. P. & Ducoste, J. J. 2016 Structural characteristics and development of the cake layer in a dynamic membrane bioreactor. *Separation and Purification Technology* **167**, 88–96.

Xu, W., Chen, Q. & Ge, Q. 2017 Recent advances in forward osmosis (FO) membrane: chemical modifications on membranes for FO processes. *Desalination* **419**, 101–116.

Yang, H. C., Liao, K. J., Huang, H., Wu, Q. Y., Wan, L. S. & Xu, Z. K. 2014 Mussel-inspired modification of a polymer membrane for ultra-high water permeability and oil-in-water emulsion separation. *Journal of Materials Chemistry A* **2** (26), 10225–10230.

Yang, H. C., Luo, J. Q., Lv, Y., Shen, P. & Xu, Z. K. 2015 Surface engineering of polymer membranes via mussel-inspired chemistry. *Journal of Membrane Science* **483**, 42–59.

Yang, H. C., Wu, M. B., Li, Y. J., Chen, Y. F., Wan, L. S. & Xu, Z. K. 2016a Effects of polyethyleneimine molecular weight and proportion on the membrane hydrophilization by codepositing with dopamine. *Journal of Applied Polymer Science* **133** (32), 43792.

Yang, Z., Wu, Y. C., Wang, J. Q., Cap, B. & Tang, C. Y. Y. 2016b In situ reduction of silver by polydopamine: a novel antimicrobial modification of a thin-film composite polyamide membrane. *Environmental Science & Technology* **50** (17), 9543–9550.

Yuan, B., Wang, X. H., Tang, C. Y., Li, X. F. & Yu, G. H. 2015 In situ observation of the growth of biofouling layer in osmotic membrane bioreactors by multiple fluorescence labeling and confocal laser scanning microscopy. *Water Research* **75**, 188–200.

Yusuf, A., Sodiq, A., Giwa, A., Eke, J., Pikuda, O., De Luca, G., Di Salvo, J. L. & Chakraborty, S. 2020 A review of emerging trends in membrane science and technology for sustainable water treatment. *Journal of Cleaner Production* **266**, 121867.

Zhang, C. Q., Hu, Z. Q. & Deng, B. L. 2016a Silver nanoparticles in aquatic environments: physiochemical behavior and antimicrobial mechanisms. *Water Research* **88**, 403–427.

Zhang, X. Y., Tian, J. Y., Ren, Z. J., Shi, W. X., Zhang, Z. B., Xu, Y. P., Gao, S. S. & Cui, F. Y. 2016b High performance thin-film composite (TFC) forward osmosis (FO) membrane fabricated on novel hydrophilic disulfonated poly(arylene ether sulfone) multiblock copolymer/polysulfone substrate. *Journal of Membrane Science* **520**, 529–539.

Zhu, Z. G., Wu, P., Liu, G. J., He, X. F., Qi, B. Y., Zeng, G. F., Wang, W., Sun, Y. H. & Cui, F. Y. 2017 Ultrahigh adsorption capacity of anionic dyes with sharp selectivity through the cationic charged hybrid nanofibrous membranes. *Chemical Engineering Journal* **313**, 957–966.

Zhu, J. Y., Hou, J. W., Zhang, Y. T., Tian, M. M., He, T., Liu, J. D. & Chen, V. 2018 Polymeric antimicrobial membranes enabled by nanomaterials for water treatment. *Journal of Membrane Science* **550**, 173–197.

First received 30 November 2022; accepted in revised form 31 March 2023. Available online 13 April 2023